# Glycoconjugate Nanoribbons from the Self-Assembly of Carbohydrate−Peptide Block Molecules for Controllable Bacterial Cell Cluster Formation

Yong-beom Lim,† Somi Park,† Eunji Lee,† Haemi Jeong,† Ja-Hyoung Ryu,† Myeong Sup Lee,‡ and Myongsoo Lee*,†

*Center for Supramolecular Nano-Assembly and Department of Chemistry, and Department of Biochemistry, Yonsei University, Seoul 120-749, Korea*

*Received January 24, 2007; Revised Manuscript Received March 20, 2007*

We demonstrate here the rational design strategy to control the length of 1-dimensional $\beta$-sheet peptide nanoassembly. We synthesized the $\beta$-sheet peptides with attached coils and carbohydrates. We reasoned that the bulkiness of the coils affects the final length of the assembled $\beta$-sheet peptide nanostructures because of the steric crowding effect. The nanostructure from the peptide with a small and linear coil was several micrometers long, whereas the one from the peptide with a high-volume-fraction dendritic coil was only about 150 nm long. For potential biological applications of the peptide nanoassemblies, we investigated the interactions of the carbohydrate-coated nanoassemblies with *E. coli* cells containing cognate binding proteins. The results showed that both of the nanoassemblies could immobilize and/or aggregate bacterial cells. The degrees of immobilization were similar for both nanoassemblies; however, only the long nanoribbon was shown to induce the formation of bacterial clusters.

## Introduction

Self-assembly, a powerful approach for the construction of novel supramolecular architectures, is mediated by noncovalent interactions, including hydrogen bonds, electrostatic interactions, and hydrophobic interactions.[1−5] Block molecules that mimic lipid amphiphilicity have been promising scaffolds for self-assembly into nanometer-sized objects with desired functions. Depending on the molecular structure of the amphiphilic components, it has been possible to construct various supramolecular architectures, such as spherical micelles, vesicles, fibers, and nanotubes.

Peptide-based self-assembling systems are increasingly used for the construction of supramolecular structures. Peptide-based assemblies, compared to organic or polymeric molecules, have advantages due to the biocompatibility and wide structural diversity of amino acids. The driving forces underlying the peptide assemblies are mostly α-helical, $\beta$-sheet, and hydrophobic interactions. Among them, the $\beta$-sheet mediated assemblies are suitable for generating 1D fiber-like nanostructures in which the peptides stack on top of each other.[6−12] In addition to the studies on naturally occurring $\beta$-sheet peptides such as $\beta$-amyloid peptides, artificially designed sequences have been developed.[8−12] The design principles for the artificial peptide sequences have mostly been the alternating placement of positively charged, hydrophobic, and negatively charged amino acids. Attraction between oppositely charged amino acids and solvophobic interactions between hydrophobic amino acids are the driving force for the proper $\beta$-sheet hydrogen bonding arrangement.

In many examples of $\beta$-sheet peptides, the interaction between pre-assembled nanostructures resulted in the formation of a hierarchy of supramolecular structures, tapes (single-molecule thick), ribbons (double tapes), fibrils (stacks of ribbons), and fibers (entwined fibrils).[13] Fibril or fiber formation is induced by lateral aggregation of the tapes or the ribbons and is sometimes advantageous when considering the formation of peptide hydrogels. However, discrete nanostructures with uniform diameter are necessary for many biological applications that need soluble and controllable materials. It has been reported that the attachment of the nonionic polymer poly(ethylene glycol) (PEG) to the $\beta$-sheet peptide could inhibit the formation of lateral aggregates.[14−17] It might also be necessary to control the length of the peptide nanostructures for some specific applications, but this has not been reported to our knowledge.

In this communication, we synthesized peptide-based block molecules that consist of a functional carbohydrate block, a coil block, and a $\beta$-sheet peptide block. We anticipated that the block molecule with a relatively small and linear coil block would form long nanostructures, whereas the molecule with a bulky dendritic coil block would form short nanostructures because of steric crowding. It has been shown, for example, in our rod−coil self-assembly system, that the bulkiness or the relative volume fraction of the rod and coil segments affects the final size and morphology of the nanostructures.[18−21] The hydrophilic carbohydrate and coil blocks would prevent the formation of lateral aggregates as well. The resulting nanostructures are discrete and coated with the functional carbohydrates. We investigated the interaction of the $\beta$-sheet peptide nanostructures with the bacterial cells.

## Experimental Section

**Materials.** Fmoc-amino acids with standard protection groups and Rink amide MBHA resin were purchased from Novabiochem. For the

* To whom correspondence should be addressed. E-mail: mslee@yonsei.ac.kr.

† Center for Supramolecular Nano-Assembly and Department of Chemistry.

‡ Department of Biochemistry.

10.1021/bm0700901 CCC: $37.00 
Published on Web 03/31/2007

construction of pDsRed, the DsRed2 gene was amplified from pDsRed2-1 (clontech) by PCR using a pair of primers (5′-CGCGGATCCAAGAAGGAGATATACATATGGCCTCCTCCGAGAAC-3′ and 5′-CCGGAATTCTTACAGGAACAGGTGGTGG-3′). The amplified fragment was restriction digested with BamH1 and EcoRI. The GFPuv gene was removed from pGFPuv (clontech) using BamH1 and EcoRI, and the PCR-amplified DsRed2 fragment was inserted instead. *E. coli* ORN178-GFP and ORN208-RFP strains were prepared by transforming ORN178 and ORN208 strains with pGFPuv and pDsRed, respectively.

**Synthesis of GP1 and GP2.** Detailed synthetic schemes and methods are given in Supporting Information. Briefly, the block peptides were synthesized on Rink amide MBHA resin using the Fmoc solid-phase peptide/organic synthesis protocol. After the construction of the block peptides on the resin, they were cleaved from the resin by treatment with cleavage cocktail (trifluoroacetic acid/ethanedithiol/thioanisole; 95:2.5:2.5) for 3 h and were triturated with *tert*-butyl methyl ether. The block peptides were purified by reverse-phase HPLC (water/acetonitrile with 0.1% TFA). The molecular weight was confirmed by MALDI-TOF mass spectrometry.

**TEM and AFM.** For TEM measurements, 3 $\mu$L of an aqueous solution of sample was placed onto a holey carbon-coated copper grid, and 3 $\mu$L of a 2% (w/w) uranyl acetate solution was added for negative stain. The sample was deposited for 1 min, and the excess solution was wicked off by filter paper. The dried specimen was observed with a JEOL-JEM 2010 instrument operating at 120 kV. The data were analyzed with DigitalMicrograph software. For AFM, 1 $\mu$L of an aqueous solution of sample was deposited onto a freshly cleaved mica surface and dried in air. The images were obtained in tapping mode with a Nanoscope IIIa instrument (Digital Instruments). AFM scans were taken at 512 × 512 pixel resolution with setpoint at 0.8−1 V and scanning speed at 1−2 Hz.

***E. coli* Motility Inhibition and Agglutination Assay.** An overnight culture of *E. coli* strain ORN178 was diluted to a concentration of $5 \times 10^7$ cells/mL with phosphate-buffered saline (PBS). Two microliters of the *E. coli* solution was placed onto a glass slide, and 2 $\mu$L of serially diluted solutions of the nanoribbons in water were added. The sample was covered with a coverglass, and a layer of rubber cement was placed around the edges. *E. coli* was observed with a Nikon Eclipse TE2000-U inverted fluorescence microscope equipped with a DXM1200C digital camera. For the motility inhibition assay, time-lapse images obtained for each concentration of nanoribbons were analyzed using Adobe Premiere software, and the ratio of nonmobile and mobile cells was calculated. The percent motility inhibition was expressed as (number of nonmobile cells/number of total cells) × 100. The agglutination index (AI) was calculated from 10 random fields of microscopic images (920 $\mu$m × 690 $\mu$m), where the number of cells in close contact were counted and averaged.

## Results and Discussion

**Design and Self-Assembly of Block Peptides.** We designed block peptides that consist of a carbohydrate mannose block, a coil block, and a $\beta$-sheet peptide assembly block (Figure 1a). Glycopeptide 1 (GP1) has a small and linear coil block and glycopeptide 2 (GP2) a bulky dendritic coil block. We anticipated that increasing the volume fraction occupied by the carbohydrate and coil block relative to the peptide block would interfere with the repetitive $\beta$-sheet growth of the peptide block because of steric crowding, thereby resulting in the premature termination of nanostructure growth. The molecules were synthesized using solid-phase peptide/organic synthesis methods. The artificially designed peptide sequence (FKFEFKFE) is known to form stable $\beta$-sheets in solution. Molecular dynamics simulations have shown that the bilayered ribbon is the most stable structure of the peptide.[11]

The formation of supramolecular assembly was investigated by circular dichroism (CD), infrared spectroscopy (IR), dynamic light scattering (DLS), transmission electron microscopy (TEM), and atomic force microscopy (AFM). The CD spectrum of GP1 showed a pronounced minimum at 215 nm, indicative of $\beta$-sheet formation (Figure 1b). IR and DLS data revealed that GP1 forms an antiparallel $\beta$-sheet and self-assembles well in solution (Supporting information). Figure 2a shows a micrograph obtained from a 0.01 wt % aqueous solution of GP1 cast onto a TEM grid. The negatively stained sample with uranyl acetate clearly shows 1D objects with a uniform width of 5 nm. Most of the strands have lengths on the order of micrometers. We were not able to exactly measure the length of the GP1 nanoribbon as it extended beyond the boundary of the TEM image at this high-resolution image. The fully extended molecular length of an 8-residue peptide in $\beta$-sheet conformation is estimated to be ~2.8 nm from molecular modeling, and thus, the 5-nm width is consistent with an antiparallel packing of peptide molecules. An examination of the 1D structures by AFM revealed their average height of 1.7 nm, indicating a ribbon-like shape (Figure 2b). The 1.7 nm height is comparable to the calculated height of a $\beta$-sheet bilayer stacked in a face-to-face manner, presumably driven by hydrophobic and $\pi-\pi$ stacking interactions of the phenylalanine residues. On the basis of these results, the peptide molecules can be considered to self-assemble into 1D ribbon-like aggregates with dimensions of 5 × 1.7 nm and lengths of several micrometers (Figure 2c). The inner core of the nanoribbons is composed of bilayered $\beta$-sheet peptide domains, and the outer edges contain mannoses and triethylene glycol segments. Within the core, the peptide segments are stacked perpendicular to the long ribbon axis with an antiparallel $\beta$-sheet arrangement.

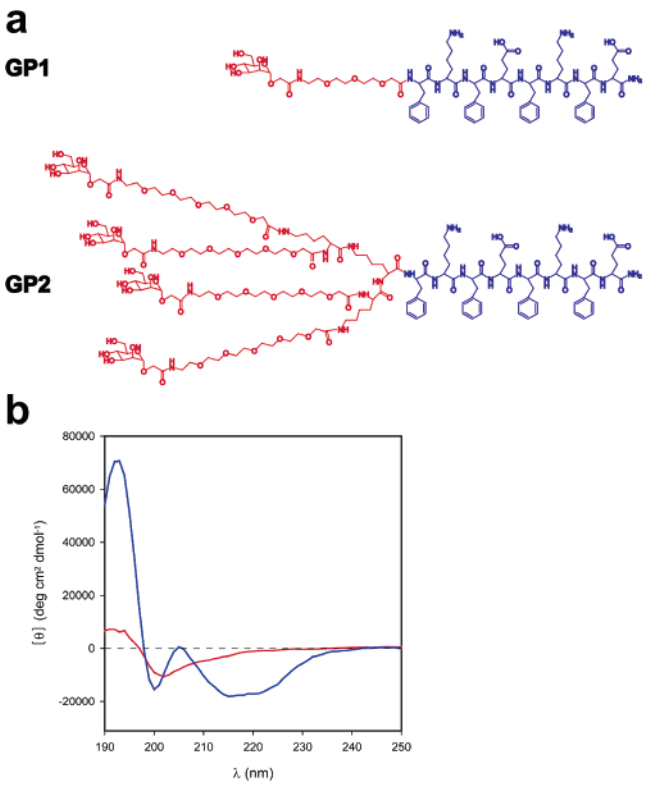


**Figure 1.** Supramolecular building blocks. (a) Structures of block peptides. (b) CD spectra of GP1 (blue) and GP2 (red).

The CD spectrum of GP2 showed that the $\beta$-sheet interaction is much weakened, indicating that the bulky dendritic block interferes with $\beta$-sheet packing and growth (Figure 1b). The IR spectrum of GP2 revealed that antiparallel $\beta$-sheet structure coexists with some other secondary structures, and the DLS

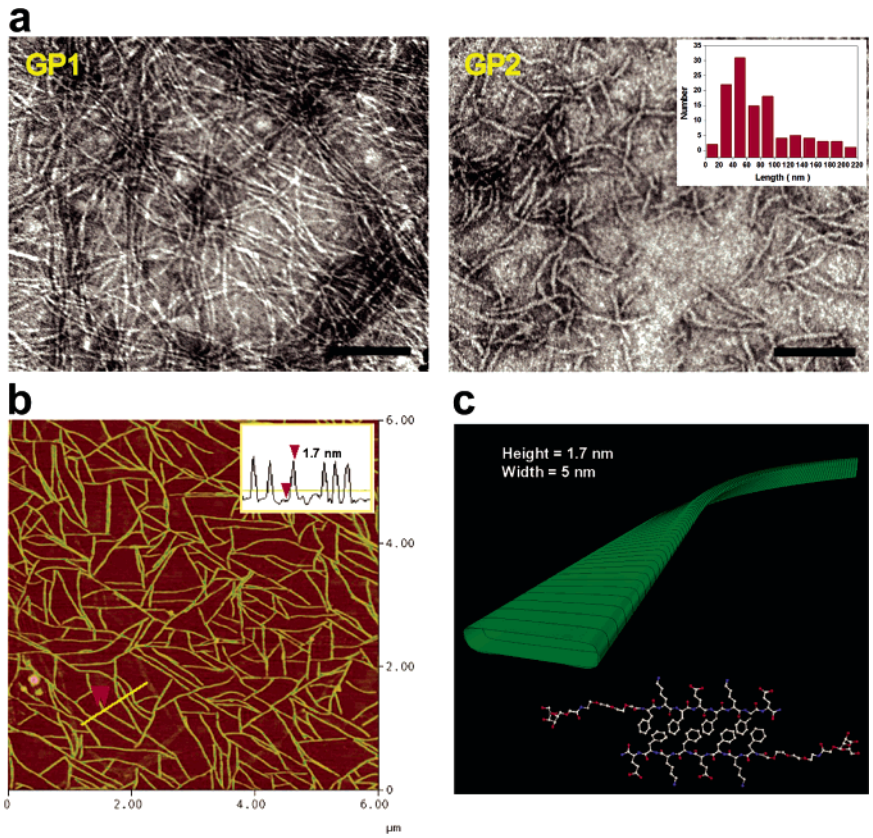


**Figure 2.** Morphologies of nanoribbons. (a) Negatively stained transmission electron micrographs of GP1 and GP2. Inset in the GP2 image: Length distribution of GP2 nanoribbons. The scale bars represent 100 nm. (b) AFM image of GP1. Inset: Height information of GP1 nanoribbons. (c) Assembly model of the GP1 nanoribbon.

spectrum showed that GP2 self-assembles well in solution (Supporting information). TEM investigations of GP2 revealed the formation of discrete 1D objects 7 nm in width (Figure 2a). The length distribution of GP2 nanoribbons was from ca. 10 nm to ca. 200 nm. The decrease in length can be interpreted as follows: The steric crowding in the dendritic coil resulted in the premature termination of ribbon growth. The increase in width is in agreement with the fact that the molecular length of GP2 is longer than that of GP1. AFM revealed discrete nanostructures with an average height of 2.3 nm (Supporting Information). The combination of spectroscopic and microscopic data leads to the conclusion that GP2 self-assembles into discrete nanoribbons with finite dimensions of 7 × 2.3 nm and a length of ∼150 nm.

**Interaction of the Peptide Nanoribbons with *E. coli* Cells.** To investigate interactions between the mannose-coated nanoribbons and the cells, we chose an *E. coli* strain with mannose-binding adhesin FimH in its type 1 pili (ORN178).[22] The type 1 pili are filamentous proteinaceous appendages produced by many members of gram-negative bacteria. The interactions would occur in a multivalent manner because both interacting partners have multiple binding molecules. It is well known that the association in multivalent binding mode is significantly tighter than that in monovalent binding mode.[23−25] To investigate the effect of the nanoribbons on the cognate *E. coli* strain ORN178, the nanoribbons were added to *E. coli*, and the effect on *E. coli* was observed by optical microscope.

As the concentration increased, the bacteria gradually lost their motility, and complete inhibition of motility took place at 2.5 $\mu$M for both nanoribbons (Figure 3a). GP1 had a slightly higher degree of motility inhibition than GP2. However, the remarkable difference between GP1 and GP2 was found with

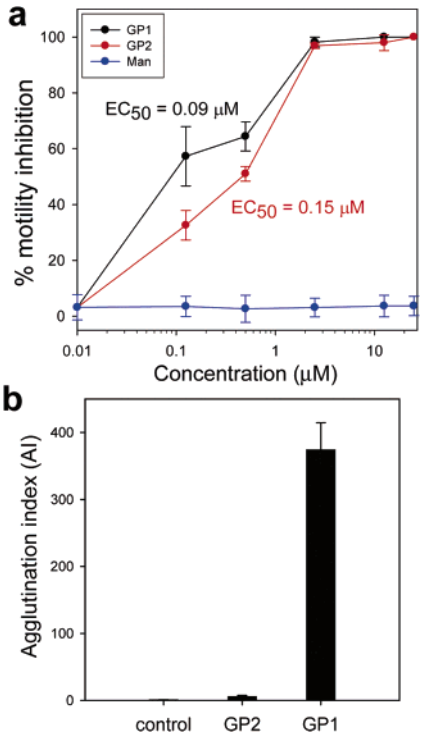


**Figure 3.** Effect of mannose-coated nanoribbons on bacterial motility and agglutination. (a) Bacterial motility inhibition assay. Each value represents the mean ± SD ($n = 3$). (b) Quantitation of the degree of agglutination as represented by the agglutination index (AI). Each value represents the mean ± SD from two independent experiments. Control; Man, GP1, and GP2 concentrations were 200 $\mu$M in terms of mannose residues.

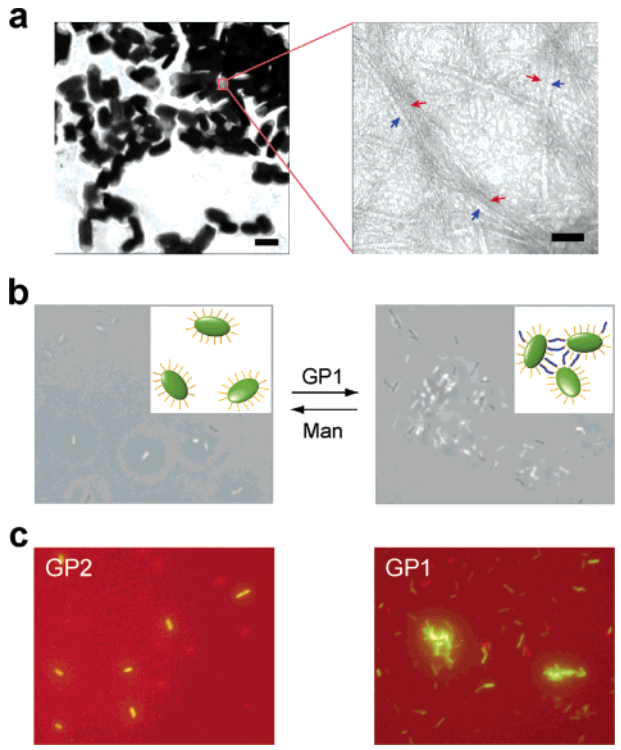


**Figure 4.** Interactions of the nanoribbons with *E. coli*. (a) TEM image of *E. coli* ORN178 strain treated with GP1. Blue and red arrows indicate type 1 pili (thicker cylindrical structures) and GP1 nanoribbons (thinner cylindrical structure), respectively. Scale bar: left (1 $\mu$m), right (50 nm). (b) Phase-contrast microscopic images of bacterial agglutination. The addition of GP1 (200 $\mu$M) to *E. coli* ORN178 resulted in motility inhibition and agglutination. Magnification: 400×. (c) Overlaid fluorescence microscopic images of bacterial agglutination with GP2 or GP1. ORN178-GFP *E. coli*, green; ORN208-RFP *E. coli*, red. Magnification: 400×.

*E. coli* agglutination ability. When the concentration of GP1 reached 100 $\mu$M, some bacteria began to form densely populated bacterial clusters (Figure 3b, Figure 4, and Supporting Information movies). In great contrast, GP2 was not able to form bacterial clusters even at very high concentrations (4 mM; in terms of mannose concentration). Quantitative measurement of the degree of agglutination showed that GP2 had a significantly lower agglutination ability than GP1 (Figure 3b). Motility inhibition and agglutination occurred immediately after the two components were mixed.

TEM investigations of the ORN178 strain incubated with GP1 showed that the nanoribbons of GP1 bound in parallel arrangement to the lateral side of type 1 pili interconnecting one another, which accounts for the agglutination phenomenon (Figure 4a). This observation is in line with previous electron microscopic evidence indicating that FimH proteins are located at the lateral side of the type 1 pili as well as at the tip.[20,26] We were not able to observe any sign of disagglutination even after several days of incubation, demonstrating the high stability of GP1 in the agglutinates.

These results demonstrate that the length of nanoribbons has a significant influence on the formation of bacterial clusters. For the glycopeptide nanoribbons to agglutinate large bacterial cells, they should be long enough, probably at least a micrometer, to interconnect pili among bacteria, as evidenced by the experiment with GP1. However, the short nanoribbons formed by GP2 seem to interconnect pili present only within a single bacterium. Intrabacterial pili aggregation might interfere with the motion of the flagella, which accounts for the inhibition of *E. coli* motility by these glycopeptide nanoribbons.

To examine the reversibility of *E. coli* agglutination, we added specific competitors (α-methyl-D-mannopyranoside; Man) in high excess (1000×) to the agglutinated solution. After the addition of excess Man, the bacterial cells were completely redispersed back into their original mobile state, demonstrating reversible agglutination (Figure 4b). In the control experiments where D(+)-galactose, a nonspecific competitor, was used to replace the bound multivalent ligands under essentially the same experimental conditions, no apparent disagglutination behavior was observed.

*E. coli* strain ORN208, an *fimH* gene mutant in which mannose binding ability of FimH was inactivated, neither lost its motility nor was agglutinated by the addition of GP1. These results indicate that multiple mannoses on GP1 mediate cross-linking of pili among bacteria through specific interactions. Specificity was further confirmed using transformed ORN178 and ORN208 strains with green fluorescent protein (GFP) and red fluorescent protein (RFP), respectively. When GP1 was added to the mixed population of ORN178-GFP and ORN208-RFP strains, only the cognate ORN178-GFP strain stopped moving and agglutinated (Figure 4c).

In conclusion, we have prepared $\beta$-sheet peptide nanoribbons displaying multiple mannose ligands on the surfaces. We were able to control the length of the 1D nanoribbons with the rational design of self-assembly building blocks, and this control produced differential biological effects of the resulting nanoribbons. This study demonstrates that the size and morphology of nanostructures are one of the most important factors in developing nanomaterials for use in biological applications. These peptide-based nanostructures are biocompatible and may be utilized in biological applications such as pathogen capture and clearance.

**Acknowledgment.** We gratefully acknowledge the National Creative Research Initiative Program of the Korean Ministry of Science and Technology for the financial support of this work.

**Supporting Information Available.** An AFM image of GP2 nanostructures, IR spectra, DLS spectra, synthesis, and movies on *E. coli* motility inhibition and agglutination. This material is available free of charge via the Internet at http://pubs.acs.org.

## References and Notes

(1) Percec, V.; Dulcey, A. E.; Balagurusamy, V. S.; Miura, Y.; Smidrkal, J.; Peterca, M.; Nummelin, S.; Edlund, U.; Hudson, S. D.; Heiney, P. A.; Duan, H.; Magonov, S. N.; Vinogradov, S. A. *Nature* **2004**, *430*, 764−768.
(2) Lehn, J. M. *Proc. Natl. Acad. Sci. U.S.A.* **2002**, *99*, 4763−4768.
(3) Ligthart, G. B.; Ohkawa, H.; Sijbesma, R. P.; Meijer, E. W. *J. Am. Chem. Soc.* **2005**, *127*, 810−811.
(4) Hartgerink, J. D.; Beniash, E.; Stupp, S. I. *Science* **2001**, *294*, 1684−1688.
(5) Zhang, S. G. *Nat. Biotechnol.* **2003**, *21*, 1171−1178.
(6) Dolphin, G. T.; Dumy, P.; Garcia, J. *Angew. Chem., Int. Ed.* **2006**, *45*, 2699−2702.
(7) Baldwin, A. J.; Bader, R.; Christodoulou, J.; MacPhee, C. E.; Dobson, C. M.; Barker, P. D. *J. Am. Chem. Soc.* **2006**, *128*, 2162−2163.
(8) Fishwick, C. W. G.; Beevers, A. J.; Carrick, L. M.; Whitehouse, C. D.; Aggeli, A.; Boden, N. *Nano Lett.* **2003**, *3*, 1475−1479.
(9) Hentschel, J.; Krause, E.; Börner, H. G. *J. Am. Chem. Soc.* **2006**, *128*, 7722−7723.
(10) Holmes, T. C.; de Lacalle, S.; Su, X.; Liu, G. S.; Rich, A.; Zhang, S. G. *Proc. Natl. Acad. Sci. U.S.A.* **2000**, *97*, 6728−6733.
(11) Marini, D. M.; Hwang, W.; Lauffenburger, D. A.; Zhang, S. G.; Kamm, R. D. *Nano Lett.* **2002**, *2*, 295−299.
(12) Matsuura, K.; Murasato, K.; Kimizuka, N. *J. Am. Chem. Soc.* **2005**, *127*, 10148−10149.
(13) Aggeli, A.; Bell, M.; Carrick, L. M.; Fishwick, C. W.; Harding, R.; Mawer, P. J.; Radford, S. E.; Strong, A. E.; Boden, N. *J. Am. Chem. Soc.* **2003**, *125*, 9619−9628.

(14) Collier, J. H.; Messersmith, P. B. *Adv. Mater.* **2004**, *16*, 907−910.
(15) Burkoth, T. S.; Benzinger, T. L. S.; Jones, D. N. M.; Hallenga, K.; Meredith, S. C.; Lynn, D. G. *J. Am. Chem. Soc.* **1998**, *120*, 7655−7656.
(16) Rosler, A.; Klok, H. A.; Hamley, I. W.; Castelletto, V.; Mykhaylyk, O. O. *Biomacromolecules* **2003**, *4*, 859−863.
(17) Eckhardt, A.; Groenewolt, M.; Krause, E.; Börner, H. G. *Chem. Commun.* **2005**, 2814−2816.
(18) Lee, M.; Cho, B. K.; Zin, W. C. *Chem. Rev.* **2001**, *101*, 3869−3892.
(19) Lee, M.; Cho, B. K.; Jang, Y. G.; Zin, W. C. *J. Am. Chem. Soc.* **2000**, *122*, 7449−7455.
(20) Kim, B. S.; Hong, D. J.; Bae, J.; Lee, M. *J. Am. Chem. Soc.* **2005**, *127*, 16333−16337.
(21) Yang, W. Y.; Ahn, J. H.; Yoo, Y. S.; Oh, N. K.; Lee, M. *Nature Mater.* **2005**, *4*, 399−402.
(22) Harris, S. L.; Spears, P. A.; Havell, E. A.; Hamrick, T. S.; Horton, J. R.; Orndorff, P. E. *J. Bacteriol.* **2001**, *183*, 4099−4102.
(23) Choi, S.-K. *Synthetic Multivalent Molecules: Concepts and Biomedical Applications*; Wiley-Interscience: Hoboken, NJ, 2004.
(24) Mammen, M.; Choi, S. K.; Whitesides, G. M. *Angew. Chem., Int. Ed.* **1998**, *37*, 2755−2794.
(25) Gestwicki, J. E.; Kiessling, L. L. *Nature* **2002**, *415*, 81−84.
(26) Lin, C. C.; Yeh, Y. C.; Yang, C. Y.; Chen, C. L.; Chen, G. F.; Chen, C. C.; Wu, Y. C. *J. Am. Chem. Soc.* **2002**, *124*, 3508−3509.

BM0700901